

RESEARCH PAPER

Fabrication of Dye-sensitized Solar Cells and Synthesis of CuNiO₂ Nanostructures Using a Photo-irradiation Technique

Amal Fadhil Kamil ¹, Hussein Ismail Abdullah ¹, and Ahmed Mahdi Rheima ^{2*}

¹ Department of Chemistry, College of Science, Mustansiriyah University, Baghdad, Iraq

² Department of Chemistry, College of Science, University of Wasit, kut, Iraq

ARTICLE INFO

Article History:

Received 05 July 2021

Accepted 18 December 2021

Published 01 January 2022

Keywords:

Binary CuNiO₂

Copper oxide

DSSCs

Nickle oxide

UV-Irradiation

ABSTRACT

The synthesis method of nanomaterials, their shape, and sizes, is essential in improving the efficiency of the dye-sensitized solar cell by increasing energy absorption and conversion. In this work, metal oxide nanoparticles included: copper oxide (CuO), nickel oxide (NiO), and binary CuNiO₂, were successfully synthesized via a photolysis method using UV lamp. Morphological, structural, optical, and electrical characterization were done using various techniques such as X-ray diffraction (XRD), field emission scanning electron microscope (FE-SEM), transmitted electron microscope (TEM), Energy-dispersive X-ray spectroscopy (EDX) and, photoluminescence spectroscopy (PL). X-ray diffraction analysis confirmed that the synthesized metal oxide nanoparticles were formed. The average particle size copper oxide (CuO), nickel oxide (NiO), and binary CuNiO₂ were rang 4-17 nm estimated by TEM. The optical properties were analyzed using photoluminescence spectroscopy (PL), and the bandgaps of CuO, NiO, and CuNiO₂ nanoparticles were determined to be 2.83 eV, 3.4 eV and 2.04 eV Sequentially. We used photochemically synthesized CuO, NiO, and CuNiO₂ nanoparticles to make dye-sensitized solar cells (DSSCs). In this research, two counter electrodes have been used: Graphene oxide Nano-Sheets and Graphene oxide\silver nanocomposite were synthesized by Modifying Hummers presses. Cibacron Brilliant Red B is one of the dyes used at the Wasit Governorate textile factory. The remainder is mostly discarded as wastewater used as a photosensitizer in our research. From the J - V curves, where efficiency ranged from 0.231 to 9.61 %, to 100 mW/cm², the opening circuit voltage (Voc), the short t current density (Jsc), the fill factor (FF) and efficiency (h) was calculated. Finally, CuO, NiO, and CuNiO₂ nanoparticles can be proven to increase the efficiency of dye-sensitized Solar Cells with brilliant B-dye cibacrons.

How to cite this article

Fadhil Kamil A, Ismail Abdullah H, Mahdi Rheima A. Fabrication of Dye-sensitized Solar Cells and Synthesis of CuNiO₂ Nanostructures Using a Photo-irradiation Technique J Nanostruct, 2022; 12(1):144-159. DOI: 10.22052/JNS.2022.01.014

INTRODUCTION

Dye-sensitized solar cell (DSSC) is a potential alternative to traditional silicon solar cells that efficiently leverages a wide-border nanocrystalline semistate (metal oxide) porous electrode property [1]. Due to the various advantages, like the cheap

price performance, lower processing costs, low incident light strength, mechanical strength, lightweight and attractive, transparent design, it is the main clean and green energy source. Nanoscience is an evolving science that attracts scientists from all walks of life to focus on it. This

* Corresponding Author Email: arahema@uowasit.edu.iq



science has high expectations and enormous potential, and it has become the most exciting and critical area [1,2]. Semiconductor oxides were already improved in recent years to achieve the properties needed for their intended applications [3]. To boost the efficiency of these oxides, specific methods such as doping and hybridization were used [4]. One of the methods is the synthesis of single-dimensional nanostructures [5]. According to research, the addition of a second metal oxide raises the light collection spectrum, leading to more electron pairs. Metals like nickel, copper, lanthanum, and vanadium, for improved catalysis, have been doped in TiO₂ [6,7]. Finally, a composite material with enhanced properties is built into its network with a semiconductor's oxide [8]. Increasing the charge separating of the composite material [9-11] can solve electron-hole recombination. The Composite has enhanced physical-chemical properties compared with each material when a narrow bandgap semiconductor oxide nanomaterial is blended with a wide bandgap semiconductor material [12]. Lead-based dielectric materials in the microelectronics industry are widely used [13]. The non-stoichiometric composition of the high temperatures of dielectron-based plum materials, such as Li, Na, Ti, Al, and CaCu₃Ti₄O₁₂ compounds [14], substituted them with plum-free materials [14]. CuO is a p-type, narrow bandgap (E_g = 1.2-1.7 eV) semiconductor used in heterogeneous catalysis, solar cells or lithium-ion battery applications among the different transitional metal oxides [14,15]. For example, nickel oxides' chemical stability and power properties in a cubic structure are commonly recognized (E_g = 3.6-4 eV, for example). Applied to gas sensors, solar cells, photocatalysis and photovoltaic devices [16], the anti-ferroir magnetic properties of nickel oxide and the high temperature of Néel (T_N = 525 K). The advancement of clean and renewable energy technologies plays an essential role in energy demand, global warming and fossil fuel depletion [17,18]. The transformation of renewable energy into electricity through Solar Cells is one of the best technologies[19-21]. With rapid development, low costs, and environmental advantages, photo-sensitive solar cells replace traditional silicon-based solar cells [22,23]. The broad prospects for the replacement of silicon solar cells are for photosensitive solar cells [24,25]. The performance of modern photosensitive solar

cells has been competitive with the production of nanostructured halves, high-performance sensitivity sensors, and robust electrolytes [26-28]. The manufacture of new photovoltaic cells in the photo-sensitive solar cell market is advanced by simple processing, cheap materials, and various applications [29]. Copper oxide (CuO) and nickel oxide (NiO) is considered a good inorganic material [30,31]. As electrons enter the empty conduction band from the valence band, the nanocomposite begins to absorb photon energy in the Hali conductor [32,33]. The electrons are stimulated, and the valence band rises, forming electron and hole pairs (e- and h+) [34]. This study reported using CuNiO₂ nanostructures synthesized by UV-Irradiation technique (novel method) as a photoanode with an organic dye (cibacron brilliant red B dye) by Recycle dye waste textile factory and use it as a Photo-sensitizer To increase the efficiency of the solar cell.

MATERIALS AND METHODS

Synthesis of CuO Nanoparticles

All chemicals were used purchased from british drug houses (BDH) and without any purification. CuO nanoparticles have been prepared by photo irradiation method, irradiation cell, as in Fig. 1 was used to irradiate copper nitrate as sources of copper oxide nanoparticles. Immersed UV source (125 W mercury medium pressure lamp) is used with maximum light intensity at 365 nm. The cell contains a quartz tube like a jacket for immersion UV source in the solution of copper nitrate. Pyrex tube is used as a reactor. An ice bath cools the reactor to avoid rising temperatures due to UV irradiation [35]. Accordingly, 30 ml of 0.02 mole urea is added slowly (drop by drop) to 30 ml, 0.01 mole Cu(NO₃)₂ under magnetic stirrer for 10 min at 30 °C. Then, the solution is irradiated by a photocell for 30 min. The blue powder is precipitate; it is separated and washed several times with deionized water. The precipitate has dried for one hour at 110°C and calcined at 400°C for 3h. A black precipitate of copper oxide nanoparticles is obtained.

Synthesis of NiO Nanoparticles

To synthesise NiO Nanoparticles, 30 ml of a 0.02 mole of urea is added slowly (one drop per second) to 30 ml, 0.01 mole Ni(NO₃)₂ with a magnetic stirrer at 30 °C. then, the solution is irradiated by photocell for 30 min. Light green powder is

precipitate; it is separated and washed several times with deionized water. The precipitate has dried for one hour at 110°C and calcined at 400°C for 3h. A black-grey precipitate of Nickel oxide nanoparticles is obtained.

Synthesis of binary CuNiO₂ Nanoparticles

Binary CuNiO₂ Nanoparticles was synthesis by the same method. Accordingly, 30 ml, 0.01 mole Cu(NO₃)₂ was mixed with 30 ml, 0.01 mole Ni(NO₃)₂ as stoichiometric ratio (1:1). Then, 60 ml, 0.02 mole of urea is added slowly (drop by drop) to the mixture and kept stirred at 30 min for 15 min. after that, the solution is irradiated by photocell for 30 min. Binary superposition is precipitated as a blue-green (dark) powder; it is separated and washed several times with deionized water (all steps done with centrifuge then decantation). The precipitate has dried in an oven at 100°C for 3 h and calcined at 400°C for 3 h. A blue-green precipitate CuNiO₂ nanoparticles have been obtained.

Synthesis of Graphene oxide and Graphene oxide\ Silver nanosheets

The modified Hammer method synthesized the graphene oxides (GO) nano-sheets. Accordingly, 2 gm of graphite powder and 0.5g of sodium nitrate (NaNO₃) were mixed with 50 ml of Sulfuric acid (H₂SO₄ 98%). The mixture was placed in the ice bath to remain at a temperature below 5 °C and kept stirring for 30 minutes. Next, 5 g of potassium permanganate (KMnO₄) was added slowly to the mixture. After 15 h, 500 ml of distilled water was added under intense stirring. Then, 10 ml of 32% hydrogen peroxide (H₂O₂) was added to the mixture. A multi-step purification procedure was

applied to isolate the reaction product. It was centrifuged, cleaned, and submerged in deionized water and an HCl (20) % solution for several steps. In the end, the black-brown product was dried at room temperature overnight to obtain graphene oxide Nano-Sheets [36].

To synthesis Graphene oxide\Silver (GO-Ag) nanosheet, 1 gm of GO nano-sheets was dispersed in 40 ml of de-ionized water. Then, 20 ml of silver nitrate (0.5 N) was added with an ice bath. The mixture continued to stir for 30 minutes, after which it was slowly added 25 ml, 1 N of sodium citrate, with kept stirring for 6 hours. Finally, the brown powder was separated and washed with de-ionized water several times and dry it at room temperature to obtain GO /Ag nanocomposites [37].

Fabrication of Dye-sensitized solar cell

Indium tin oxide coated glass (ITO with an 85 % transmitted and 7 Ohm Resistant) washed several times with acetone, purified water in an ultrasonic bath to eliminate impurity, and dried with an air blower. A dye-sensitized solar cell (15*20*1 mm) was Prepared according to Mixing the nano oxides powder (0.3 g) and ethanol (10 ml) in a colloidal solution of CuO, NiO, and CuNiO₂ nanostructures. The photo-anode was taken with a dropper on the conductive side to cover the colloid solution for 45 min in the air, then annealed at 150°C for 30 minutes[38]. The nanostructure oxides electrode is cooled and saturated with 0.5 M dye solution (cibacron brilliant red B) for 6 h. A conductive side counter electrode covers graphene oxide nano-sheets. The electrolyte solution (I⁻/I⁻³) was penetrated by capillary action from the anode to

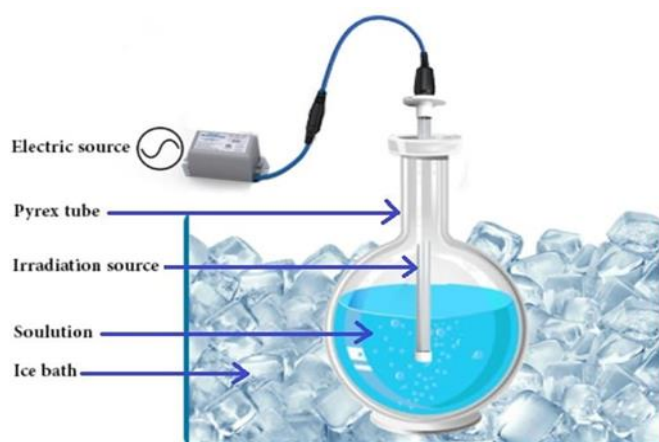


Fig .1. photo-chemical Immersed UV cell

the counter electrode. The two electrodes were kept using binding clips. And same steps again but used graphene oxide/ silver nanocomposite as the cathode electrode for all of (CuO, NiO, and CuNiO₂) nanostructure.

RESULTS AND DISCUSSIONS

Some techniques have been used to Characterize CuO, NiO, and CuNiO₂ samples. X-ray diffraction (XRD) Model D-5000 was used

to investigate the composition of the specimens by using Cu-Kα radiation (λ=0.154nm) source in θ/2θ. The XRD (10° to 80°) and measurement temperature (25 °C) are 2θ for each of CuO, NiO and CuNiO₂ NP_s [20]. Field emission scanning electron microscope (FE-SEM) model Jeol JSM-6010LV A total of 20 μL was lowered over a grid of 300-mesh Cu and dried at room temperature. Photoluminescence measurements (PL) emission measured for selective metal oxide to calculate the

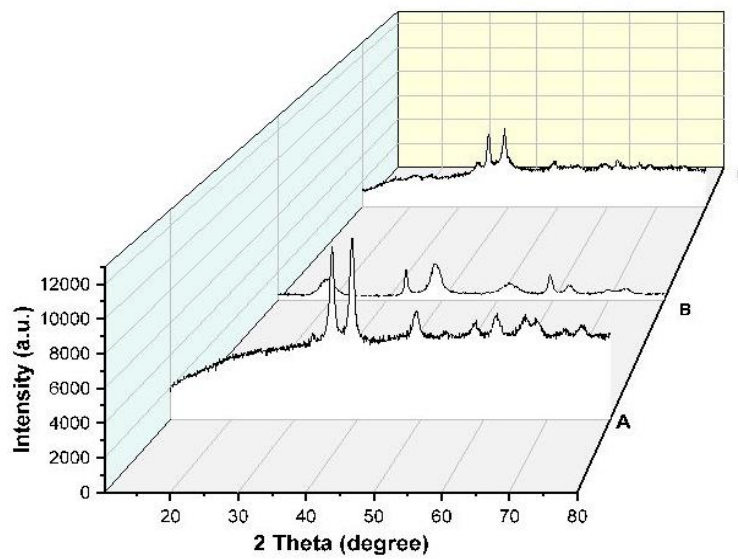


Fig. 2. XRD pattern of prepared samples before calcination A) Cu(OH)₂ B) Ni(OH)₂ and, C) binary Cu(OH)₂- Ni(OH)₂

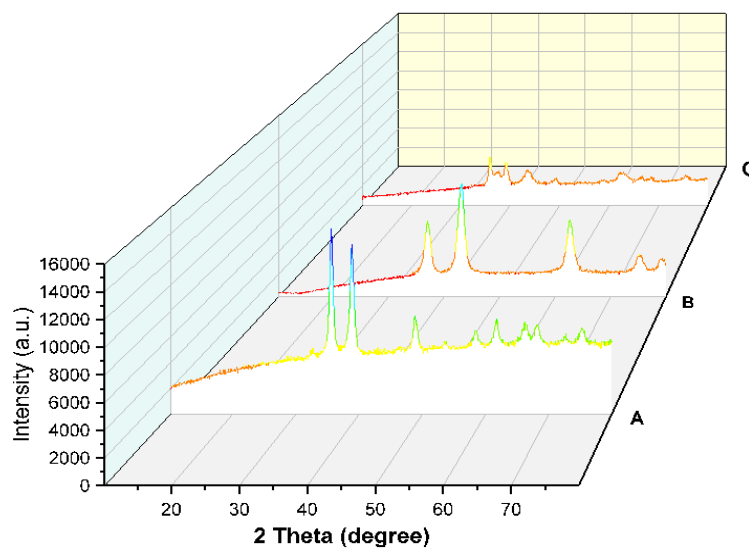


Fig. 3. XRD pattern of prepared samples after calcination at 400 °C, A) CuO B) NiO and, C) CuNiO₂ NPS

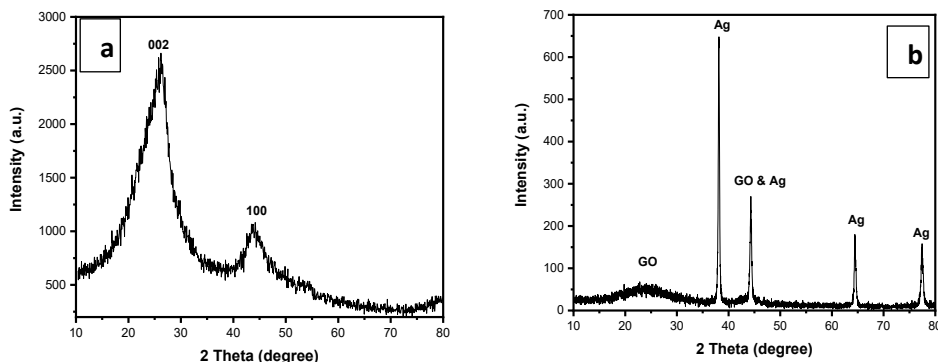


Fig. 4 XRD of a) GO Nano-sheets and b) GO-Ag nanocomposites.

energy gap of emission. A Raman spectrometer by Thermo Scientific fitted with a 532-nm laser and a 10-inch target was taken at room temperature used for GO and GO/Ag. TEM model Jeol JSM-6010LV observed sample morphologies with 500 X and 60 kX magnification with a 5kV accelerating voltage. Before TEM analyzes, the samples (GO and GO/Ag powder) were discrete in the deionized and sonic water for approximately 15 minutes.

XRD characterization of metals oxide Nanostructures

The composition of the specimens was investigated using X-ray diffraction (XRD) Model D-5000 with a Cu-K radiation (λ=0.154nm) source in 2θ. Figs. 2 and 3 depict the sample's XRD patterns Before and after calcination at 400 °C. Before calcination in Fig. 2 (A, B, and C), which agrees well with M_(n)(OH)_n. Both diffraction peaks can be indexed to the pure structure of the Cu(OH)₂ JCPDS, [files No. 13-0420], Ni(OH)₂ JCPDS, [files No. 13-0420], and binary Cu(OH)₂- Ni(OH)₂ respectively.

After calcination at 400 °C in Fig. 3 (A, B and C), The XRD pattern of CuO and NiO shows that all peak of refraction aligns perfectly with the normal refraction details for all CuO and NiO (JCPDS NO.48-1548 and JCPDS No. 78-0643 respectively). For Fig. 4, A crystalline monoclinic structure is supported by the pattern. Peaks for CuO nanoparticles at diffraction angles of 32.5°, 35.4°, 38.7°, 48.7°, 53.5°, 58.3°, which correspond to 110, 002, 111, and 202 020, 202 phases. The Diffraction pattern peaks have been observed at 37.1775, 43.1897, 62.7810, 75.2675, 79.2376 degrees, which refer to planes of (111), (200), (220), (311), and (222) linked to the cubic structure of NiO (Fig. 3 B). There are no peaks for any impurity in binary oxides (Fig 3 B), meaning that the sample is exceptionally pure. Sharp and intense peaks demonstrate typical quality crystalline CuNiO₂ by a new at 35.84 and 39.14 degrees. For determining the crystallite size, the Scherrer equation is used [20]. The crystallite size of CuO, NiO and CuNiO₂ nanoparticles were (13.36, 7.84 and 13.27) nm, respectively.

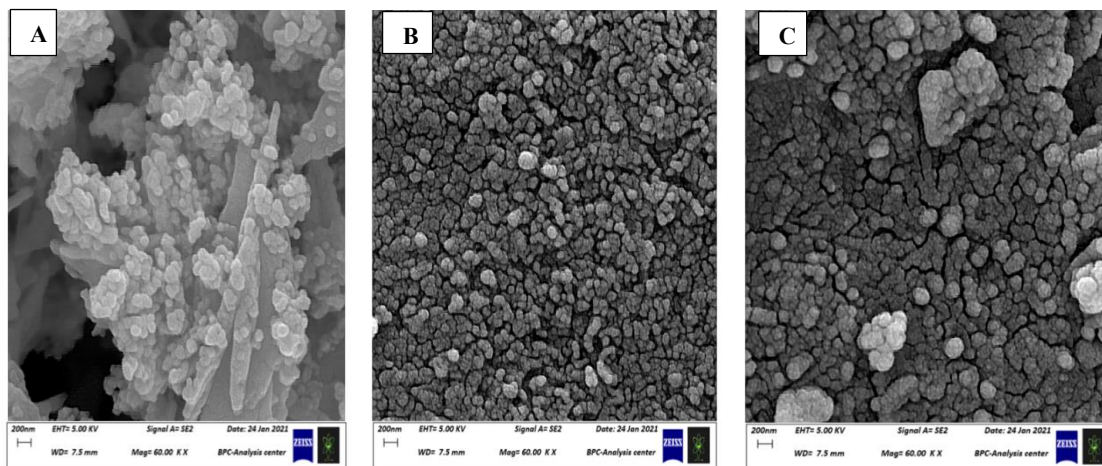


Fig. 5. FE-SEM of a) CuO, b) NiO, and c) binary CuNiO₂ nanoparticles.

On the other hand, Fig. 4 (a and b) shows the XRD pattern of graphene oxide nanosheets and graphene oxide-Ag nanocomposites. The plane matches the GO XRD pattern with a value of $2\theta = 10.19^\circ$ value that fits the plane (100). There was also a small peak at $2\theta = 20.93^\circ$, representing the plane (002). Because of functional groups containing oxygen during graphite oxidation, the spacing of the layer in Graphene oxide Nano-sheets increases in contrast to graphite. On the graphene oxide Nano-sheets -Ag nanocomposite,

a peak linked to both Graphene oxide Nano-sheets and Ag nanoparticles was observed (interlayer spacing of 1.392 nm). However, a minor shift of the peak to the lower 2θ confirms that Ag NPs are intercalated with GO sheets.

FE-SEM characterization

FE-SEM was used to investigate the surface morphology of pure CuO, pure NiO, and binary CuO-NiO nanoparticles calcined at 400 °C. (Fig. 5). The production of semi-spherical aggregates

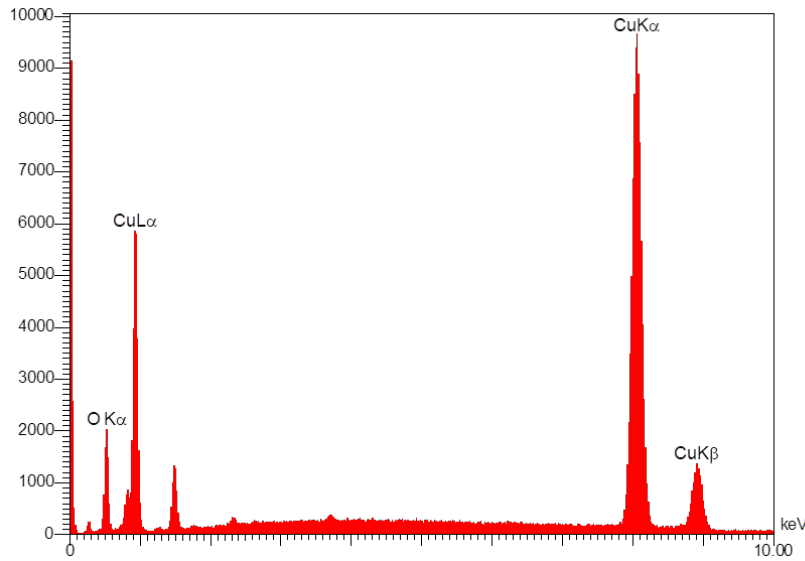


Fig. 6. EDX spectrum of CuO NPs

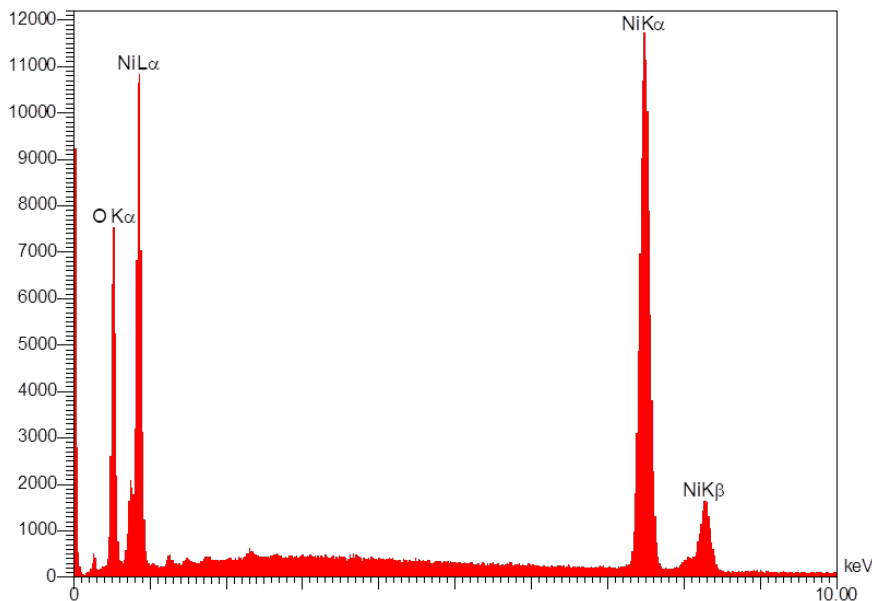


Fig. 7. EDX spectrum of NiO NPs

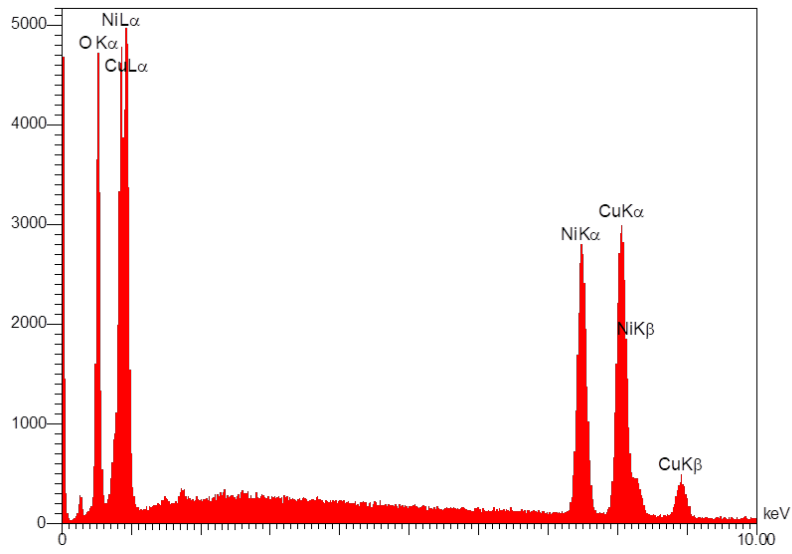


Fig. 8. EDX spectrum of CuNiO₂ NPs

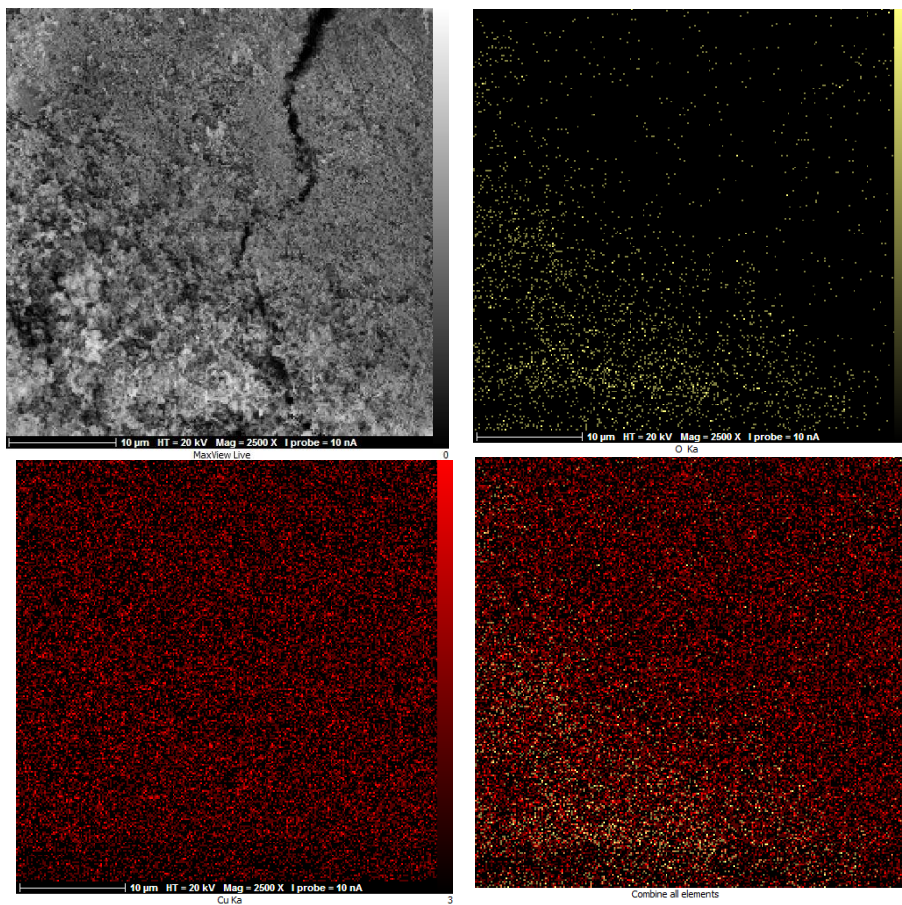


Fig. 9. EDAX- mapping of CuO NPs

as nearly uniform distribution for all prepared samples can be concluded from SEM analysis. In addition, the crystal nature of equal-sized synthesized nanoparticles is demonstrated. CuO, NiO, and CuNiO₂ nanoparticles have been discovered to have average sizes of 19 nm, 13 nm, and 21 nm, respectively, and are homogeneous with little aggregation due to their small size. These findings are nearly identical to those obtained from the Typical XRD pattern.

EDX characterization

The EDX spectrum of CuO, NiO, and CuNiO₂ nanoparticles is shown in Figs. 6, 7, and 8. Typical Nickel, Copper, and oxygen peaks are present in the spectrum. The results confirm the high purity of the synthesized nanostructures. In addition, the theoretical calculations of the elements agree with the practical estimates obtained from the

EDX measurement. Figs. 9, 10, and 11 indicate that CuO, NiO, and CuNiO₂ NPs have been spread well by the mixed catalyst's matrix. Further data indicate typical images of x-ray mapping to display the distribution of elemental components of a CuO and NiO catalyst, which will support the dispersion of the catalyst elements.

TEM spectroscopy

The TEM of CuO, NiO, and CuNiO₂ nanoparticles are shown in Figs. 12 A, B, and C. The TEM image of nanoparticles of different shapes and sizes is shown in Fig. 12. The size of the particles varied between 4 and 17 nanometers. The larger particles may result from smaller nanoparticles' agglomeration with dimensions that match the XRD analysis described. The crystallite size is measured with XRD based on the expansion of Bragg's reflections because of the number of

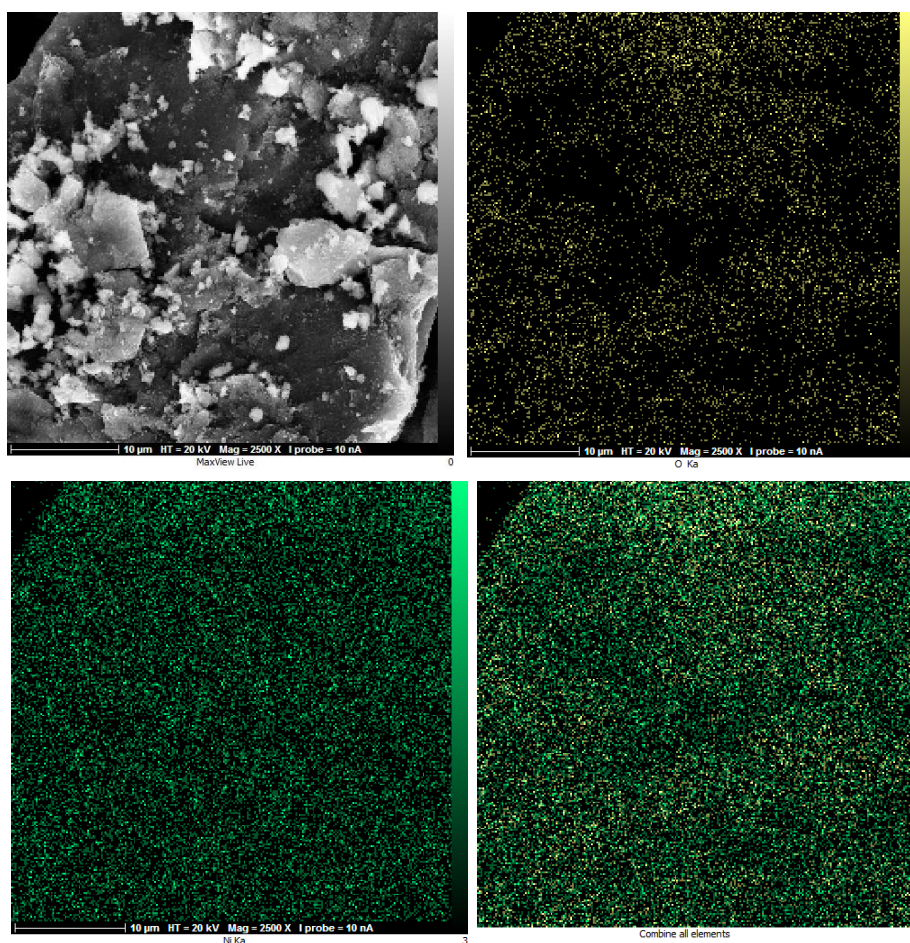


Fig. 10. EDAX- mapping of NiO NPs

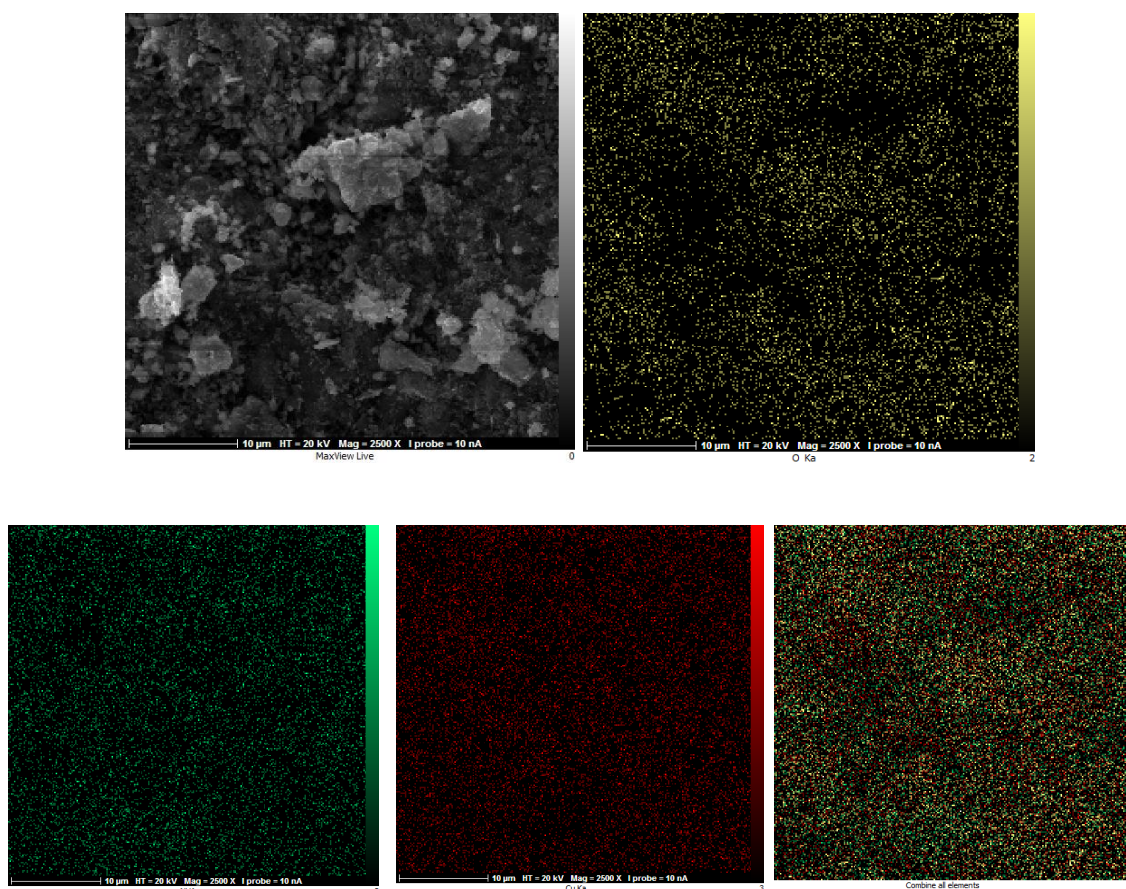


Fig. 11. EDAX-Mapping of CuNiO₂ NPs

parallel lattice planes causing diffraction. The Scherrer equation parameter k approximates the crystallite shape factor; however, the size distribution is not considered, resulting in size values different from the TEM.

Fig. 13 A and B shows different thicknesses. Dark regions represent the dense stacking nanostructures of several layers of GO and GO/Ag with certain feature groups of oxygen. The higher clarity levels indicate much thinner films of a few layers of graphene oxide \silver resulting from stacking exfoliation. GO and GO/Ag Significantly wider surface area with high delaminated graph layers transparency (about one-layer thickness). The TEM images indicate that GO sheet layers are 4 to 6 nm thicker than graphs of a single layer. The increased thickness is due to the insertion of functional groups containing oxygen that thicker and alters the GO sheet surface (Fig. 13 A). The particle size of silver on a surface of GO was less than 20 nm. Therefore, Ag nanoparticle growth's

diffusion rate could rely heavily on the number of Ag atoms given to standing clusters (Fig. 13 B). Finally, autocatalytic oxidation comprises steps 1 and 2 to absorb the remaining AgNO₃ to obtain the nanoparticles of Final Ag.

Raman spectroscopy

Fig. 14 (a and b) shows the Raman spectra of the prepared GO sheets and GO/Ag nanocomposites samples. The Raman spectra of the prepared GO sheets showed typically (a) and GO-Ag nanocomposites (b) peaks near (1355 and 1592 cm⁻¹), (1345 and 1572 cm⁻¹), respectively. Thus, Raman's shift to GO sheets and GO-Ag nanocomposites shift to the sp² region. A more clearly realized 2D splitting phenomenon is the luxurious spectrum of Fig. 14 (a and b) [36,37], in which the existence of the 2D band is visible. In comparison, the 2D band of GO plates and GO-Ag nanocomposites are more symmetric, showing that their crystallites have decreased the number

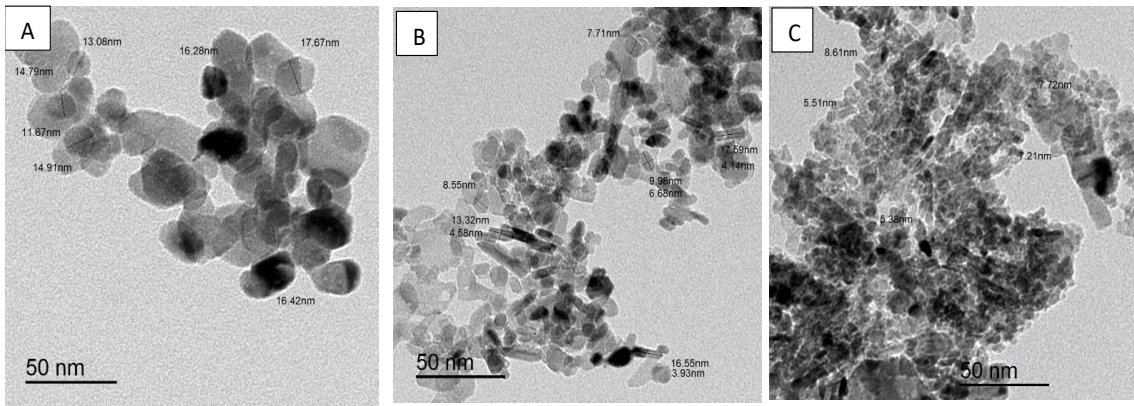


Fig. 12. TEM images of A) CuO NPs, B) NiO NPs and, C) CuNiO₂ NPs

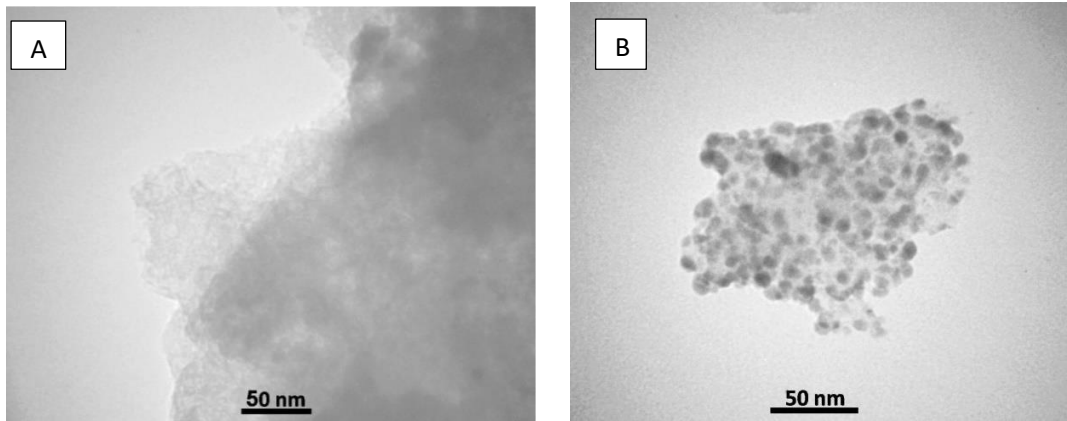


Fig. 13. TEM images of A) GO nano-sheets and B) GO/Ag nanocomposite

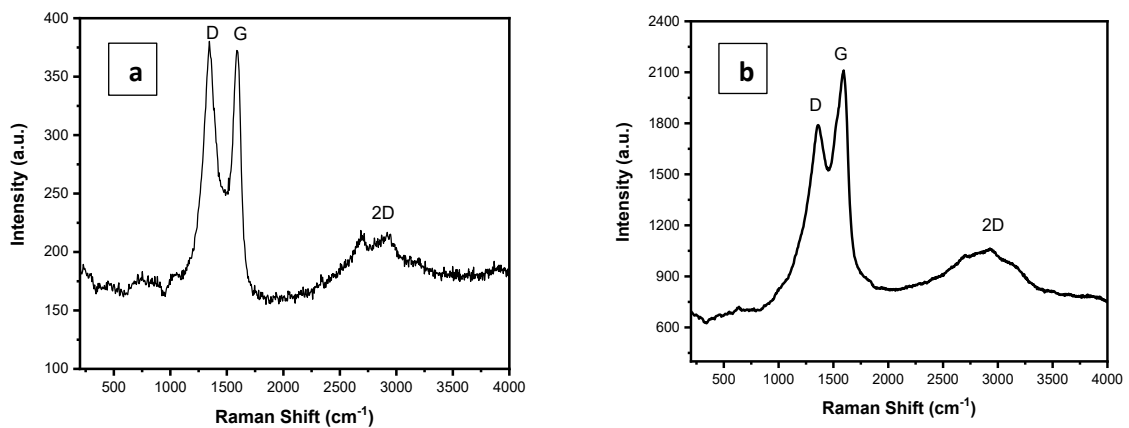


Fig. 14. Raman spectra of a) GO nano-sheets and b) GO-Ag nanocomposites.

of graphic layers. However, the 2D range of GO-Ag and GO-Ag represents a sharp and symmetrical summit. The number of layers formed through measurement is less than 3 layers, and SEM also

confirmed this.

Photoluminescence measurements (PL)

Nano-powder of CuO, NiO, and binary CuO-

NiO nanoparticles calcined at 400 oC were analyzed using a solid-state photo-luminescent (PL) spectrum (Perkin– Elmer spectrometer design LS55 with photomultiplier tube) for prepared its emissions. The behaviour of the PL spectrum is highly influenced by the size distribution of nanoparticles, which can be derived from various sources. To measure the emission energy gap, Figs. 15,16 and 17 show the fluorescence spectra of CuO, NiO, and binary CuO-NiO nanoparticles with a maximum wavelength of 437 nm, 364 nm and,

434nm, respectively. The PL spectra have a single peak in this case, with a nearly wide full width at half limit (FWHM). According to the equation $E_g (e.V) = 1240/\lambda$ [20], the energy gap was calculated to be 2.83, 3.40 and 2.04 e.V, respectively.

Dye-sensitized solar cells parameters

Figs. 18-20 shows the current density-voltage (J-V) curve of the CuO, NiO, and CuNiO₂ NPs -based DSSC. The parameters of dye-sensitized solar cells, like I_{sc}, V_{oc}, I_{max}, and V_{max}, were calculated from

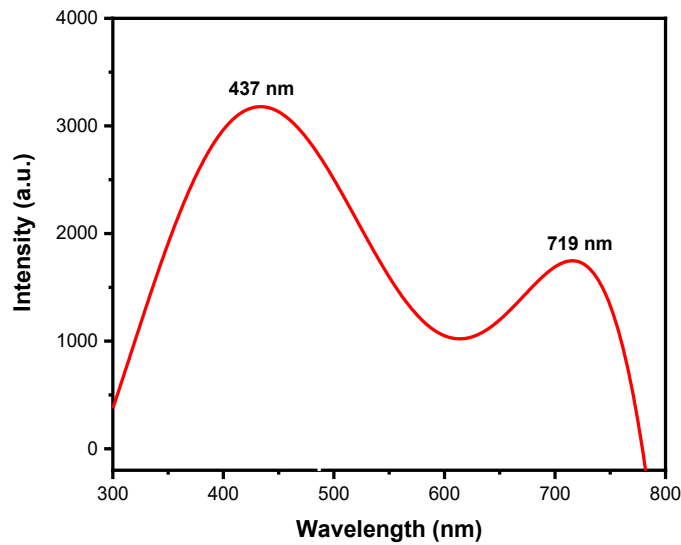


Fig. 15. The PL analysis of CuO NPs

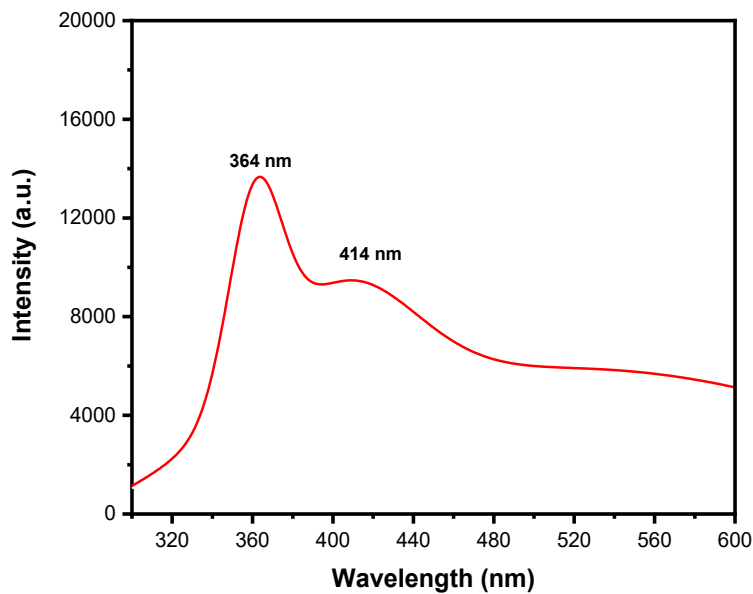


Fig. 16. The PL analysis of NiO NPs

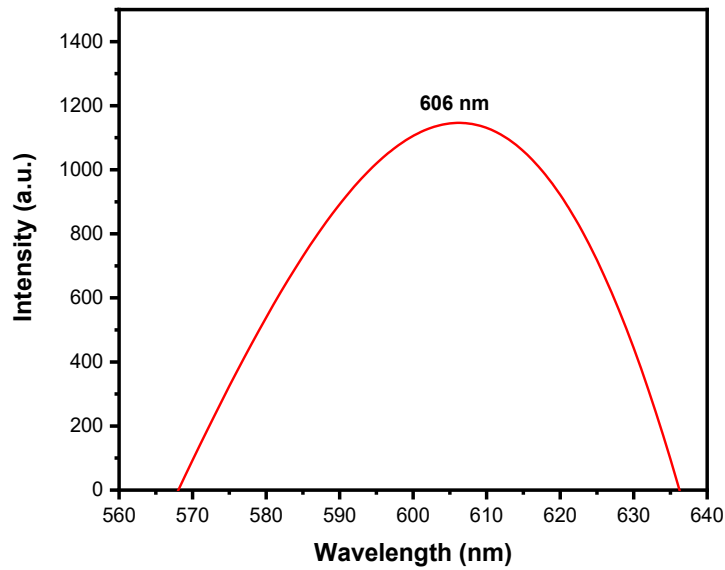


Fig. 17. The PL analysis of CuNiO₂ NPs

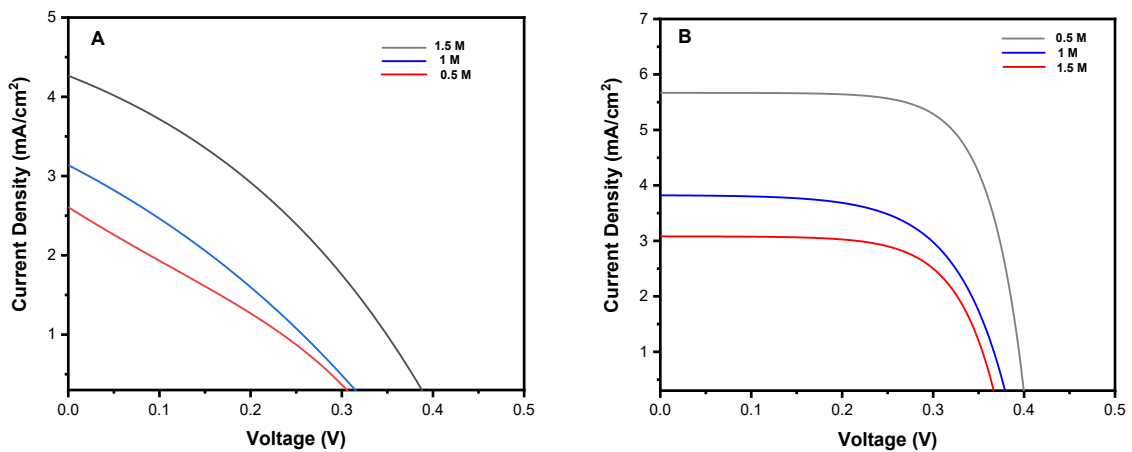


Fig. 18. J -V curves of NiO NPs-DSSC at different Concentration dye and counter electrodes A) GO and B) GO\Ag.

the J-V curves, and the fill factor and cell efficiency were determined by a solar simulator with a halogen lamp and a light intensity of 100mW/cm² using the equations [20]:

$$\eta = \frac{pm}{pin} \times 100\% \quad (1)$$

$$F.F = \frac{Jm Vm}{Jsc Voc} \quad (2)$$

Tables 1-3 show the Dye-sensitized solar cells parameters that were determined. Because of the concentration sensitizing dye and small particles

of synthesized metals oxide nanoparticles, it was critical for metals oxide nanoparticles-based Dye-sensitized solar cells parameters. This study used two counter electrodes, Graphene Nano-sheets (GO) and Graphene\Ag nanocomposite (GO-Ag). The cell's power conversion efficiency improved with higher dye concentrations in each of them (GO and GO\Ag). According to data, The cell efficiency is arranged in sequence CuNiO₂ > CuO > NiO. This arrangement can be mainly due to the gap energy of the oxides, and the increased absorption may also justify the dye molecules' high efficiency on the metal oxide nanoparticles'

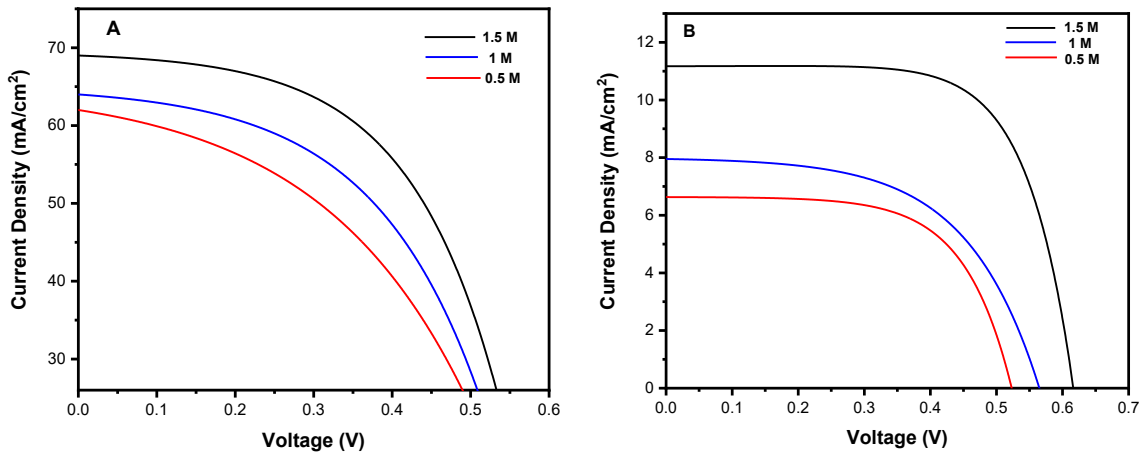


Fig. 19. J -V curves of CuO NPs-DSSC at different Concentration dye and counter electrodes A) GO and B) GO\Ag.

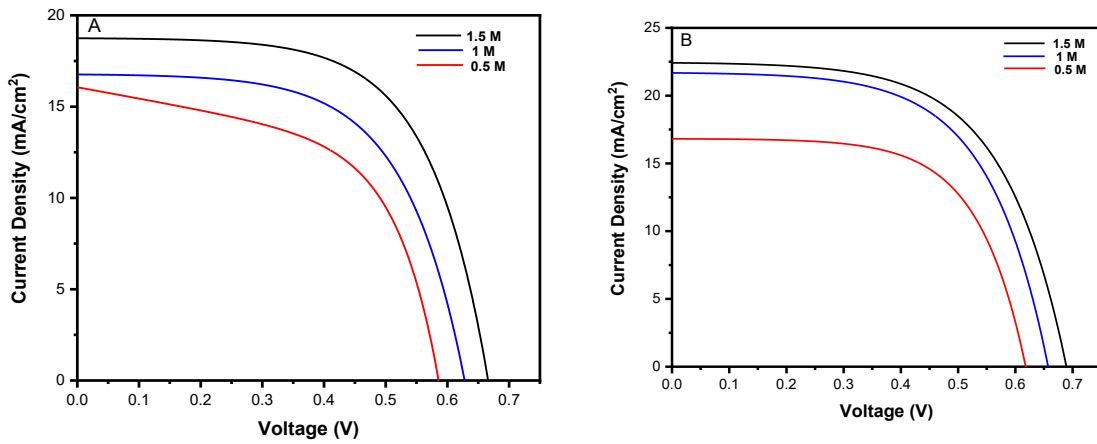


Fig. 20. J -V curves of CuNiO₂ NPs-DSSC at different Concentration dye and counter electrodes A) GO and B) GO\Ag.

Table 1. DSSC parameters of NiO NPs at different concentrations dye and counter electrodes

counter electrodes	Conc. Dye [M]	Voc (V)	J sc (A/cm ²)	V max (V)	J max (A/cm ²)	P max (W/cm ²)	F.F	η %
GO	0.5	0.33	0.0·26	0.21	0.0·11	0.0·0231	0.269	0.231
	1	0.34	0.0·32	0.22	0.0·12	0.0·0264	0.242	0.264
	1.5	0.39	0.0·42	0.23	0.0·20	0.00·460	0.280	0.460
GO\Ag	0.5	0.37	0.0032	0.28	0.0027	0.000756	0.638	0.756
	1	0.38	0.0040	0.30	0.0029	0.000870	0.572	0.870
	1.5	0.41	0.0061	0.32	0.0046	0.000147	0.588	1.470

Table 2. DSSC parameters of CuO NPs at different concentrations dye and counter electrodes

counter electrodes	Conc. Dye [M]	Voc (V)	J sc (A/cm ²)	V max (V)	J max (A/cm ²)	P max (W/cm ²)	F.F	η %
GO	0.5	0.52	0.0062	0.41	0.0043	0.00176	0.546	1.76
	1	0.53	0.0064	0.43	0.0052	0.00223	0.657	2.23
	1.5	0.55	0.0067	0.45	0.0055	0.00247	0.670	2.47
GO\Ag	0.5	0.53	0.0065	0.43	0.0057	0.00245	0.711	2.45
	1	0.58	0.0079	0.47	0.0064	0.00300	0.656	3
	1.5	0.62	0.0114	0.5	0.0098	0.00490	0.693	4.9

Table 3. DSSC parameters of CuNiO₂ NPs at different concentrations dye and counter electrodes

counter electrodes	Conc. Dye [M]	Voc (V)	J sc (A/cm ²)	V max (V)	J max (A/cm ²)	P max (W/cm ²)	F.F	η %
GO	0.5	0.59	0.0164	0.48	0.0119	0.00571	0.590	5.71
	1	0.63	0.0173	0.51	0.0131	0.00668	0.612	6.68
	1.5	0.67	0.0185	0.52	0.0167	0.00868	0.700	8.68
GO\Ag	0.5	0.62	0.0183	0.51	0.0134	0.00683	0.602	6.83
	1	0.66	0.0213	0.52	0.0172	0.00894	0.635	8.94
	1.5	0.69	0.0223	0.54	0.0178	0.00961	0.624	9.61

surface. As a result, CuNiO₂ nanoparticles are promising for future photovoltaics because the process is simple, and the materials can even be produced easily. However, the current density rating was relatively poor. The photo-current is the most important parameter for calculating the overall device efficiency limit. As particle sizes reach the nanoscale, the parent materials behave differently due to their large surface area and surface energy. When comparing the Dye-sensitized solar cells prepared by GO Nano-sheets with GO\Ag nanocomposite, we note that the efficiency was high when the electrode had GO\Ag nanocomposite. The reason was the increase in the surface area and the high conductivity that silver gave when attached to graphene, leading to greater freedom of movement of the electron and increased efficiency [38].

CONCLUSION

Finally, the photolysis method produced CuO, NiO, and CuNiO₂ NPs. According to TEM, the average particle size of the synthesized CuO, NiO, and CuNiO₂ NPs ranged from 4 to 17 nm. SEM and TEM revealed the nanoparticles' spherical appearance, with little aggregation. In PL spectroscopy, the

CuO, NiO, and CuNiO₂ NPs showed a broad surface Plasmon resonance absorption peak at max= 437, 364, and 606 nm, respectively, with energy gaps of 2.83, 3.4, and 2.04 eV. Current density-voltage behaviour under simulated sunlight was used to investigate the performance of the CuO, NiO, and CuNiO₂ DSSC. Due to a considered increase in dye absorption on the surface of CuO, NiO, and CuNiO₂, the high effectiveness of the manufactured DSSC was clear. The fabrication of DSSC at different concentrations of dye and counter electrodes using photochemically synthesized CuO, NiO, and CuNiO₂ is a promising and straightforward method for our future well-being as photo-sensitizers for the DSSC dyes released into the water as waste from textile factories are used.

CONFLICT OF INTEREST

The authors declare that there is no conflict of interests regarding the publication of this manuscript.

REFERENCE

1. Hussain D, Rheima AM, Jaber S, kadhim M. Cadmium Ions Pollution Treatments in Aqueous Solution Using Electrochemically Synthesized Gamma Aluminum Oxide Nanoparticles with DFT study. Egyptian Journal of

- Chemistry. 2020;63(2):417-424.
2. Smyrniou Z, Georgakopoulou E, Sotiriou S. Promoting a mixed-design model of scientific creativity through digital storytelling—the CCQ model for creativity. *International Journal of STEM Education*. 2020;7(1).
 3. Syama S, Mohanan PV. Microfluidic based human-on-a-chip: A revolutionary technology in scientific research. *Trends in Food Science & Technology*. 2021;110:711-728.
 4. Zhi J, Zhou M, Zhang Z, Reiser O, Huang F. Interstitial boron-doped mesoporous semiconductor oxides for ultratransparent energy storage. *Nature Communications*. 2021;12(1).
 5. Sayed DM, El-Deab MS, Allam NK. Multi-walled vanadium oxide nanotubes modified 3D microporous bioderived carbon as novel electrodes for hybrid capacitive deionization. *Sep Purif Technol*. 2021;266:118597.
 6. Hanifehpour Y, Mirtamizdoust B, Ahmadi H, Wang R, Joo SW. Sonochemical synthesis, crystal structure, and DFT calculation of an innovative nanosized Pb(II)-azido metal-organic coordination polymer as a precursor for preparation of PbO nanorod. *Chemical Papers*. 2020;74(10):3651-3660.
 7. *Responsive Nanomaterials for Sustainable Applications*. Springer Series in Materials Science: Springer International Publishing; 2020.
 8. Contreras D, Melin V, Pérez-González G, Henríquez A, González L. Advances and Challenges in BiOX (X: Cl, Br, I)-Based Materials for Harvesting Sunlight. *Environmental Chemistry for a Sustainable World*: Springer International Publishing; 2019. p. 235-282.
 9. Zheng C, Zhang C, Zhang K, Zhang J, Jin L, Asiri AM, et al. Growth of ZnFe₂O₄ nanosheets on reduced graphene oxide with enhanced ethanol sensing properties. *Sensors Actuators B: Chem*. 2021;330:129280.
 10. Murali A, Sarswat PK, Free ML. Minimizing electron-hole pair recombination through band-gap engineering in novel ZnO-CeO₂-rGO ternary nanocomposite for photoelectrochemical and photocatalytic applications. *Environmental Science and Pollution Research*. 2020;27(20):25042-25056.
 11. Ahmadi M, Seyed Dorraji MS, Hajimiri I, Rasoulifard MH. The main role of CuO loading against electron-hole recombination of SrTiO₃: Improvement and investigation of photocatalytic activity, modeling and optimization by response surface methodology. *J Photochem Photobiol A: Chem*. 2021;404:112886.
 12. Xing H, E L, Guo Z, Zhao D, Liu Z. Enhancement in the charge transport and photocorrosion stability of CuO photocathode: The synergistic effect of spatially separated dual-cocatalysts and p-n heterojunction. *Chem Eng J*. 2020;394:124907.
 13. Siva Prakash R, Mahendran C, Chandrasekaran J, Marnadu R, Maruthamuthu S, Yahia IS, et al. A facile fabrication of Sn-doped CeO₂ nanocrystalline thin films with enhanced photodiode properties for optoelectronic applications. *Appl Phys A*. 2021;127(3).
 14. J P, Kottam N, A R. Investigation of photocatalytic degradation of crystal violet and its correlation with bandgap in ZnO and ZnO/GO nanohybrid. *Inorg Chem Commun*. 2021;125:108460.
 15. Arjunkumar B, Ramalingam G, Ramesh M, Ponraj JS, Rao KV. Investigation of uni-directional nanorods composed microspheres and branched TiO₂ nanorods towards solar cell application. *Mater Lett*. 2020;273:127900.
 16. Arjun Kumar B, Ramalingam G, Karthigaimuthu D, Elangovan T, Vetrivelan V. Fabrication of natural dye sensitized solar cell using tridax procumbens leaf and beetroot extract mixer as a sensitizer. *Materials Today: Proceedings*. 2022;49:2541-2545.
 17. Blessi S, Anand S, Manikandan A, Sonia MML, Vinosel VM, Slimani Y, et al. Influence of Ni substitution on optomagnetic and electrochemical properties of CTAB-capped mesoporous SnO₂ nanoparticles. *Journal of Materials Science: Materials in Electronics*. 2021;32(6):7630-7646.
 18. Vignesh R, Arjun kumar B, Muthuvinayagam A, Elangovan T, Kaviyarasu K, Theophil Anand G, et al. Unstable cell efficiency in CdS quantum dot sensitized solar cell using low cost lugols iodine aqueous electrolyte. *Materials Today: Proceedings*. 2021;36:159-162.
 19. Gupta P, Pandey NK, Kumar K, Yadav BC. Structural, optical and LPG sensing properties of zinc-doped nickel oxide pellets operated at room temperature. *Sensors and Actuators A: Physical*. 2021;319:112484.
 20. Kadhum HA, Salih WM, Rheima AM. Improved PSI/c-Si and Ga/PSi/c-Si nanostructures dependent solar cell efficiency. *Appl Phys A*. 2020;126(10).
 21. Wang D, Yang Y, Guo T, Xiong X, Xie Y, Li K, et al. Effect of pulse bias voltages on performance of CdTe thin film solar cells prepared by pulsed laser deposition. *Solar Energy*. 2021;213:118-125.
 22. Zhang S-T, Guc M, Salomon O, Wuerz R, Izquierdo-Roca V, Pérez-Rodríguez A, et al. Effective module level encapsulation of CIGS solar cells with Al₂O₃ thin film grown by atomic layer deposition. *Sol Energy Mater Sol Cells*. 2021;222:110914.
 23. Persiani SGL. *Materials of Autoreaction*. Design Science and Innovation: Springer Singapore; 2020. p. 115-155.
 24. Sandhya M, Ramasamy D, Sudhakar K, Kadirgama K, Samykan M, Harun WSW, et al. A systematic review on graphene-based nanofluids application in renewable energy systems: Preparation, characterization, and thermophysical properties. *Sustainable Energy Technologies and Assessments*. 2021;44:101058.
 25. Ansari AA, Nazeeruddin MK, Tavakoli MM. Organic-inorganic upconversion nanoparticles hybrid in dye-sensitized solar cells. *Coord Chem Rev*. 2021;436:213805.
 26. Nguyen TT, Patel M, Kim S, Mir RA, Yi J, Dao V-A, et al. Transparent photovoltaic cells and self-powered photodetectors by TiO₂/NiO heterojunction. *J Power Sources*. 2021;481:228865.
 27. Pulli E, Rozzi E, Bella F. Transparent photovoltaic technologies: Current trends towards upscaling. *Energy Convers Manage*. 2020;219:112982.
 28. De Tommasi E, Esposito E, Romano S, Crescitelli A, Di Meo V, Mocella V, et al. Frontiers of light manipulation in natural, metallic, and dielectric nanostructures. *La Rivista del Nuovo Cimento*. 2021;44(1):1-68.
 29. Ates M, Yilmaz E, Tanaydin MK. Challenges, novel applications, and future prospects of chalcogenides and chalcogenide-based nanomaterials for photocatalysis. *Chalcogenide-Based Nanomaterials as Photocatalysts*: Elsevier; 2021. p. 307-337.
 30. Maslamani N, Khan SB, Danish EY, Bakhsh EM, Zakeeruddin SM, Asiri AM. Super adsorption performance of carboxymethyl cellulose/copper oxide-nickel oxide nanocomposite toward the removal of organic and inorganic pollutants. *Environmental Science and Pollution*

- Research. 2021;28(29):38476-38496.
31. Fedorov AV, Kukushkin RG, Yeletsky PM, Bulavchenko OA, Chesalov YA, Yakovlev VA. Temperature-programmed reduction of model CuO, NiO and mixed CuO–NiO catalysts with hydrogen. *J Alloys Compd.* 2020;844:156135.
 32. Beshkar F, Salavati-Niasari M, Amiri O. A reliable hydrophobic/superoleophilic fabric filter for oil–water separation: hierarchical bismuth/purified terephthalic acid nanocomposite. *Cellulose.* 2020;27(16):9559-9575.
 33. Shtan'ko V, Chinkov E, Shrayber A, Stepanov S. Intrinsic luminescence of CaF₂ crystals under simultaneous excitation of pulsed accelerated electrons and stimulated emission of semiconductor CdSSe. *Radiat Phys Chem.* 2020;168:108619.
 34. Wang X, Sun K, Gu S, Zhang Y, Wu D, Zhou X, et al. Construction of a novel electron transfer pathway by modifying ZnIn₂S₄ with α-MnO₂ and Ag for promoting solar H₂ generation. *Appl Surf Sci.* 2021;549:149341.
 35. Novel method to synthesis nickel oxide nanoparticles for antibacterial activity. *Iranian Journal of Physics Research.* 2020;20(3).
 36. Hou Y, Lv S, Liu L, Liu X. High-quality preparation of graphene oxide via the Hummers' method: Understanding the roles of the intercalator, oxidant, and graphite particle size. *Ceram Int.* 2020;46(2):2392-2402.
 37. Ikram M, Raza A, Imran M, Ul-Hamid A, Shahbaz A, Ali S. Hydrothermal Synthesis of Silver Decorated Reduced Graphene Oxide (rGO) Nanoflakes with effective Photocatalytic Activity for Wastewater Treatment. *Research Square Platform LLC*; 2020.
 38. Abdul-Ameer Aboud N, Alkayat WMS, Hussain DH, Rheima AM. A comparative study of ZnO, CuO and a binary mixture of ZnO_{0.5}-CuO_{0.5} with nano-dye on the efficiency of the dye-sensitized solar cell. *Journal of Physics: Conference Series.* 2020;1664(1):012094.